Available online at www.sciencedirect.com

ScienceDirect

Underground Space xxx (xxxx) xxx

www.elsevier.com/locate/undsp

Effects of underground explosions on soil and structures

Daniel Ambrosini [a,*], Bibiana Luccioni [b]

[a] National University of Cuyo, CONICET, Argentina
[b] National University of Tucumán, CONICET, Argentina

Abstract

Much effort has been dedicated to the study of underground explosions because they pose a major threat to people and structures below or above the ground. In this regard, it is especially important to model the propagation of blast waves in soil and their effects on structures. The main phenomena caused by underground explosive detonation that must be addressed are crater or camouflet formation, shock wave and elastic–plastic wave propagation in soil, and soil-structure interaction. These phenomena can be numerically simulated using hydrocodes, but much care must be taken to obtain reliable results. The objective of this study is to analyze the ability of a hydrocode and simple soil models that do not require much calibration to approximately reproduce experimental and empirical results related to different buried blast events and to provide general guidelines for the simulation of this type of phenomena. In this regard, crater formation, soil ejecta, blast wave propagation in soil, and their effects on structures below and above the ground are numerically simulated using different soil models and parameters; the results are analyzed. The properties of soil have a significant effect on structures, the ejecta, and the propagation of shock waves in soil. Thus, the model of the soil to study these phenomena must be carefully selected. However their effect on the diameter of a crater is insignificant.

Keywords: Shock waves; Underground explosions; Soils; Hydrocodes

1 Introduction

Blast loads have become the focus of attention because of a number of accidental and intentional events in recent years that affected important structures all over the world; this indicates that this issue must be addressed in structural designs and reliability analyses. As a consequence, extensive research based on blast loads has been conducted in the past few decades (Alia & Souli, 2006; Ambrosini, Luccioni, Danesi, Riera, & Rocha, 2002).

Dynamic loads due to explosions lead to strain rates in the order of 10^{-1}–$10^{3}\ s^{-1}$, which indicate short-time dynamic behavior of the materials involved, mainly characterized by a large overstrength and increased stiffness in comparison with normal and static properties. In the case of soils, the response and the mechanism of crater formation are particularly complex owing to the usual anisotropy and nonlinear nature of the material, the variability of their mechanical properties, and the coexistence of the three phases of soils: solid, liquid, and gas. Generally, simplification assumptions must be made to solve specific problems. For many years, most practical problems have been solved through empirical approaches. Years of industrial and military experience have been condensed in the form of charts or equations (Baker, Cox, Westine, Kulesz, & Strehlow, 1983; Smith & Hetherington, 1994). These are useful tools, for example, to establish the explosive weight to yield a perforation of certain dimensions.

With the rapid development of computer hardware over the past few decades, it has become possible to perform detailed numerical simulations of explosions on personal computers, thereby significantly increasing the availability

* Corresponding author.
E-mail addresses: dambrosini@uncu.edu.ar (D. Ambrosini), bluccioni@herrera.unt.edu.ar (B. Luccioni).

https://doi.org/10.1016/j.undsp.2019.09.002

Please cite this article as: D. Ambrosini and B. Luccioni, Effects of underground explosions on soil and structures, Underground Space, https://doi.org/10.1016/j.undsp.2019.09.002

of these methods. Developments in integrated computer hydrocodes are completing the tools necessary to successfully perform numerical analyses. Nevertheless, it is important to note that models and analysis procedures still need to be experimentally validated.

Much effort has been dedicated to the study of underground explosions because they pose a serious threat. The total number of mines across the world is estimated to be between 60 and 110 million (Cheeseman, Wolf, Yen, & Skaggs, 2006). Thus, protection devices must be designed for people and vehicles to reduce the damage caused to them by landmine blasts (Cheeseman et al., 2006). Owing to the complexity of the problem, numerical models that can help in understanding the interaction between blast products and structures and the resulting damage are required not only for damage assessment but also for the design and hardening of protection devices and vehicles.

On the other hand, the protection of essential facilities against explosions usually includes reinforced concrete structures (Wang, Lu, Hao, & Chong, 2005). Very complex phenomena including the interaction between explosives, soil, and structure are involved in the behavior of underground structures under blast loads (Wang et al., 2005). Crater or camouflet formation, shock waves, and plastic waves are also important phenomena that must be considered in the analysis of this type of events. Complex loads characterized by high intensity and short duration are produced by explosions. Their effects strongly depend on the size, shape, and type of explosives; the depth at which an explosive is buried; the location of the detonation point; the type, density, and water content of soil (Cheeseman et al., 2006).

When a high-impact explosive is detonated, an internal wave is developed in the explosive, and a shock wave is generated that propagates through the surrounding medium. This flow is fairly complex, and it involves physical phenomena that include burning effects and heat transfer (Alia & Souli, 2006). Blast-wave propagation through soil and its effect on structures below or above the ground are strongly dependent on soil properties. The resulting problem is geometrically and physically highly non-linear (Wang et al., 2005). Addressing all these issues in one simple model is challenging, but it can be very useful in reducing the number of required tests and analyzing their results. After validation with experimental results, such numerical tool can help in improving the design of protection systems and structures.

In this study, we numerically simulate different buried blast events and analyze the crater formation, soil ejecta, blast wave propagation in soil, and the effect on structures above and below the ground. The ability of simple soil models that do not require much calibration to approximately reproduce experimental and empirical results is checked. Moreover, the influence of soil parameters on the effect of buried explosives is also addressed.

The crater dimensions defined by Kinney and Graham (1985) are used in this study (Fig. 1). In Fig. 1, D is the apparent crater diameter measured from the loose soil mounts around the crater, D_r is the actual crater diameter, and H_2 is the apparent depth of the crater.

2 Theory and state of the art

2.1 Crater formation

A cavity is always formed when a confined explosion is produced in a mass of soil. If the explosion is close to the surface, a crater is formed and a complex interaction between gravity effects, soil strength, and transient load conditions develops. The most important variables in defining the crater shape and size are the mass W of the explosive and the depth of the detonation beneath the air/-soil interface d. For underground explosions, the crater formation mechanism is altered by gravitational effects. When the depth of the detonation increases, larger amounts of

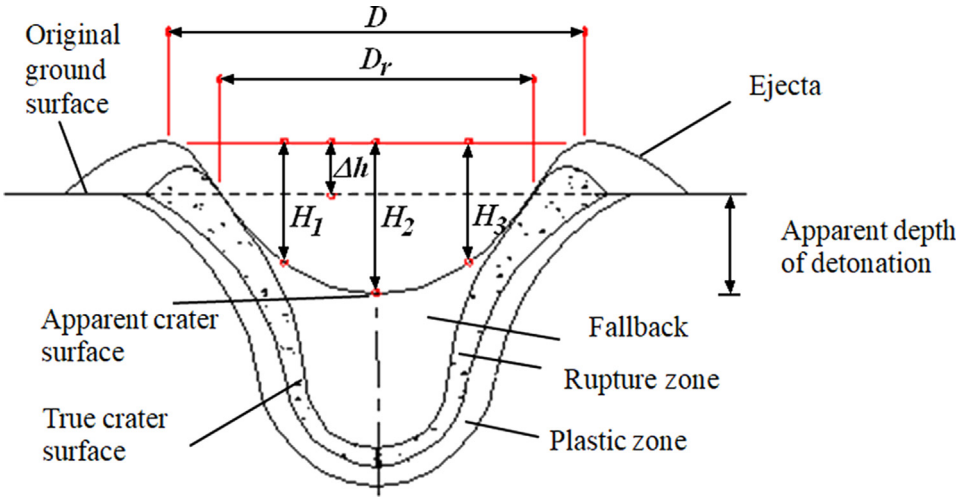

Fig. 1. Conventional crater.

Please cite this article as: D. Ambrosini and B. Luccioni, Effects of underground explosions on soil and structures, Underground Space, https://doi.org/10.1016/j.undsp.2019.09.002

subsoil must be expelled by the explosion. Thus, the crater radius and the depth increase when d increases, until a certain threshold value, above which they rapidly decrease (Bull & Woodford, 1998).

Studies concerned with the characteristics of craters formed by explosions usually resort to dimensional analyses and statistics. According to the scaling law, any linear dimension L of the crater can be expressed as a constant multiplied by W^{α} divided by the distance of the charge from the ground, where W represents the equivalent TNT mass of explosive and α is a coefficient dependent on whether the gravitational effects can be neglected or not. If the gravitational effects can be neglected, the cubic root law is applicable ($\alpha = 0.33$), otherwise, the functional dependence can be quite complex.

Baker, Westine, and Dodge (1991) presented a dimensional study to model the crater formation phenomenon in the case of underground explosions. Six parameters were chosen to define the problem: the explosive mass W, the depth of the explosive charge d, the apparent crater radius R, the soil density ρ, and two strength parameters to define the soil properties, one with the dimensions of stress σ, related to the soil strength, and the other with the dimensions of a force divided by a cubic length (Nm^{-3}) K, which considers gravitational effects.

After a dimensional analysis and many empirical observations, the following functional relation was obtained (Baker et al., 1991).

$$\frac{R}{d} = f\left(\frac{W^{\frac{7}{24}}}{\sigma^{\frac{1}{6}} K^{\frac{1}{8}} d}\right) \tag{1}$$

By plotting $\frac{R}{d}$ (scaled radius of the crater) as a function of $W^{\frac{7}{24}}/d$ (Baker et al., 1991), it can be seen that this relation is consistent with experimental results and can be approximately simplified by two straight lines, one with a moderate slope for $\left(W^{\frac{7}{24}}/d\right) > 0.3$ and one with a steeper slope for $\left(W^{\frac{7}{24}}/d\right) < 0.3$. For $\left(W^{\frac{7}{24}}/d\right) < 0.3$, the scaled radius of the crater is sensitive to small changes in the independent parameter and consequently, the independent parameter or the scaled radius may exhibit great variability. The experimental conditions are better controlled for $\left(W^{\frac{7}{24}}/d\right) > 0.3$.

It can be deduced (Baker et al., 1991) that the specific weight ρg is the best measure for K and that ρc^2 is the best measure for σ, where c is the seismic velocity in the soil. If experimental results for different types of soils are plotted in a $\frac{R}{d}$ versus $\frac{W^{\frac{7}{24}}}{\rho^{\frac{7}{24}} c^{\frac{1}{3}} g^{\frac{1}{8}} d}$ graph, it can be clearly seen that there is very little variability in the results.

The scale depth, defined as $\lambda_c = d/W\left(\mathrm{m \cdot kg^{-\frac{1}{3}}}\right)$, can be used to differentiate blast effects on soils. When $0.2\ \mathrm{m \cdot kg^{-\frac{1}{3}}} < \lambda_c < 0.8\ \mathrm{m \cdot kg^{-\frac{1}{3}}}$ (Fig. 1) a conventional crater is developed; when $0.8\ \mathrm{m \cdot kg^{-\frac{1}{3}}} < \lambda_c < 1.39\ \mathrm{m \cdot kg^{-\frac{1}{3}}}$ a partial camouflet is obtained, whereas a camouflet is formed for $\lambda_c > 1.39\ \mathrm{m \cdot kg^{-\frac{1}{3}}}$ (Bull & Woodford, 2004). The camouflet is a spherical void surrounded by highly compacted subgrade and with a conical volume composed of loose soil that has been moved upwards and resettled above it.

Recently, Wang, Qiu, and Yue (2018) derived a scaling law for cratering explosions in multi-layered media subjected to underground explosions.

2.2 Effects of buried explosions on structures

The effect of buried explosions on structures strongly depends on the position of the structures relative to the source of the explosion. A number of studies have been performed in the general area of blast response of structures over the years. However, the loading mechanisms from explosive blast-soil-structure interaction such as those occurring from the detonation of a buried mine below a vehicle are poorly understood at present (Rigby et al., 2016). Similarly, the entire process of load generation and the exact distribution of the load on structures located above or below the ground have not been fully characterized yet. Basically the problem can be studied both experimentally and/or numerically.

2.2.1 Experimental research and theory

Bergeron, Walker, and Coffey (1998) provided a detailed description of the physical process following the detonation of a buried explosive that can be summarized in three stages as follows (Rigby et al., 2016):

(1) Phase 1 – Detonation and early interaction with the soil;
(2) Phase 2 – Gas expansion;
(3) Phase 3 – Soil ejecta.

The loading produced during phase 2 on targets located above ground is highly localized with high magnitude and short duration. It results from a combination of the impact of ejected soil and the high pressure on the target surface. Loading during phase 3 is produced by the later soil ejecta and is more uniformly distributed (Grujicic & Pandurangan, 2008).

The destructive output of a PMN mine was experimentally assessed by Swinton and Bergeron (2004) by detonating actual mines in air and then in soil. The fragmentation pattern was recorded using a combination of flash X-rays, fragmentation packs, and gelatine cylinders. It was proved that the soil has a strong influence on the characteristics of the fragmentation and the blast produced by the mine.

Hlady (2004) demonstrated that the energy released by a mine greatly varies with the soil conditions surrounding it. Tests involving the explosion of landmines in engineered soil containers were performed. Different variables includ-

Please cite this article as: D. Ambrosini and B. Luccioni, Effects of underground explosions on soil and structures, Underground Space, https://doi.org/10.1016/j.undsp.2019.09.002

ing standoff distance, explosive overburden, and the soil type, moisture, and density were studied.

Some works, including Fourney, Leiste, Haunch, and Jung (2010), reported on reduced-scale laboratory tests using a few grams of buried explosive to evaluate the global and local impulse on plates located above the ground. They showed that explosives buried on saturated soil can produce almost twice the impulse of those buried in dry sand. Clarke, Rigby, Fay, Tyas, Reay, and Warren (2015) observed that dry sands produce more 'blast-type' loading, whereas wet sands produce more 'bubble-type' loading.

More recently, Denefeld, Heider, and Holzwarth (2017) presented a new experimental method based on a ring arrangement to evaluate the specific impulse produced by a buried explosion on a target above the ground. They used this approach to evaluate the influence of the soil type and water content and the depth of the burial on the specific impulse distribution.

Additionally, a largescale experimental method for the direct measurement of the spatial and temporal distribution of a load resulting from a buried explosion was recently developed by Rigby et al. (2016, 2018). They proved that there is a single fundamental loading mechanism when explosives are detonated in saturated soil independent from the particle size and soil cohesion and that the variability in localized loading can be attributed to the particle size distribution of the soil.

Hu, Long, Liu, Yang, and Han (2014) studied the swelling movement induced by an underground explosion of an aluminized explosive in multilayered compact material soil. The process of swelling movement was recorded by a high-speed camera and verified by two similar underground explosions experiments.

While the effect of buried explosions on structures located above the ground was experimentally investigated by several authors, experimental data concerning the effect of buried explosions on structures above or under the ground are extremely scarce (Lu, Wang, & Chong, 2005) and this type of problem has been addressed mostly numerically. Wu, Hao, Lu, and Sun (2004) and Wu and Hao (2005) analyzed the ground motion produced by underground explosions on structures located on the ground. Yankelevsky, Karinski, and Feldgun (2011) studied buried explosions and particularly, the shock wave peak pressure attenuation. They showed that the shock wave peak pressure attenuation may be well represented by a power law with a constant exponent only for certain types of soils.

2.2.2 State of the art of numerical models

Owing to the complex physics involved in the explosion of buried explosives and their effect on structures, computational methods should be used to model these types of problems. Classic soil models are not capable of representing realistically the response of materials involved under high deformation, high-deformation rate, and high-temperature conditions and thus, many authors have proposed new soil models to overcome this difficulty. Wang, Hao, and Lu (2004) formulated a numerical three-phase soil model capable of simulating explosions and blast wave propagation in soils. A new material model for sand was developed by Grujicic, Pandurangan, and Cheeseman (2006) to include the effects of the degree of saturation and the deformation rate on the constitutive response. This material model for sand was used within a non-linear-dynamics transient computational analysis to study the various phenomena associated with the explosion of shallow-buried and ground-laid mines.

Nowadays, fully coupled analyses allows taking into account soil-structure interaction. Such analyses can be carried out using the finite element method (FEM) combining Euler and Lagrange processors or using the arbitrary Lagrangian-Eulerian (ALE) method (An, Tuan, Cheeseman, & Gazonas, 2011; Grujicic et al., 2006; Jayasinghe, Thambiratnam, Perera, & Jayasooriya, 2013; Wu & Hao, 2005; Wu et al., 2004). However, it is difficult to handle this type of multiphase multiphysics problems with extremely large deformation with conventional methods. Accordingly, particle methods have been widely used to simulate the interaction of explosives and soils (Chen & Lien, 2018).

Using their model, Wang et al. (2004), Lu et al. (2005), and Wang et al. (2005) performed fully coupled numerical simulations of the response of buried concrete structures subjected to underground explosions. They employed the smooth particle hydrodynamics (SPH) technique to model the explosive charge and the close-in zones where large deformation occurred, whereas conventional FEM was used to model the remaining soil region and the buried structure. Chen and Lien (2018) also used the SPH technique to simulate the detonation of buried explosions and their effect on structures. They proved that the method can reproduce the fragmentation of soil produced by the shock wave and explosive gas expansion and the soil-structure interaction.

Recently, Fan and Li (2017) coupled the state-based Peridynamics model with a modified smooth SPH model to model soil fragmentation under buried explosions.

In this study, we verify the ability of Euler Lagrange finite element processors and simple local continuum soil models to reproduced different phenomena produced by buried explosions, such as cratering, soil ejecta, the effect on targets located above the ground, blast wave propagation in soil, and the effect on underground structures.

3 Numerical models

3.1 Numerical mesh

All the numerical analyses are performed using a hydrocode (ANSYS-AUTODYN, 2017). In all cases, the explosives are modeled as TNT, using the TNT-equivalent mass so that the results can be compared.

A Euler Godunov multi-material with strength higher-order processor (Alia & Souli, 2006) is used to model the

Please cite this article as: D. Ambrosini and B. Luccioni, Effects of underground explosions on soil and structures, Underground Space, https://doi.org/10.1016/j.undsp.2019.09.002

air, the explosive charge, and the soil. Solids such as steel plates and concrete walls are modeled using the Lagrange processor. The Euler Lagrange interaction is defined in this case. In all cases, the mesh is refined until the convergence of the results is obtained.

3.2 Boundary transmit

A transmit boundary is defined for the soil external limits when it is modeled with the Lagrange processor. The transmit boundary is used to fulfill the radiation condition, and it is only active for flow out of a grid. Flow out of soil, air, and TNT is allowed in all external limits of Euler meshes. These types of boundary conditions allow stress waves to propagate without reflection through mesh limits, simulating an indefinitely extending medium. Using them, the size of the numerical models can be reduced.

3.3 Material models

The ideal gas equation of state (EOS) is used for air, whereas the Jones-Wilkins-Lee (JWL) EOS is used for TNT. Standard material parameters available in the code are used for air and TNT (Luccioni & Ambrosini, 2006).

To study the influence of the soil model and soil properties, the four types of soil described below are defined.

A shock EOS, an elastoplastic strength model based on the Drucker Prager criterion, and a hydro tensile limit are used for Soil 1. The Mie-Gruneisen form of the EOS based on the shock Hugoniot is used. The yield stress is a piecewise linear function of pressure. A summary of the soil properties used for Soil 1 is presented in Table 1.

A linear EOS combined with an elastoplastic strength model is used for Soil 2 and Soil 3, which only differ in their elastic constants. The properties of Soil 2 and Soil 3 are presented in Table 2.

A compaction EOS combined with the Moxnes and Ødegårdstuen (MO) granular strength model is used for Soil 4, which represents dry sand. The compaction EOS is an extension of the porous EOS that allows more control over loading/unloading slopes. The MO granular model is an extension of the Drucker-Prager model that considers the effects associated with granular materials. In addition to pressure enhancement, the model also considers density hardening and variations in the shear modulus. The material properties of Soil 4 are presented in Table 3.

In the examples, steel and concrete structures are modeled using standard models for these types of materials. An elastoplastic model is used for steel, and an RHT model is used for concrete. The models are not described in this paper because they play a secondary role for the results presented, except for Section 5.4, where the properties are indicated.

Table 1
Properties of Soil 1.

Equation of State: Shock	
Strength: Drucker Prager	
Reference density $\rho = 1.92$ g/cm^3	
Gruneisen Gamma $\Gamma = 0.11$	
Initial sound speed $c_o = 1.614 \times 10^3$ m/s	
Dimensionless parameter $S = 1.5$	
Shear Modulus $G = 2.0 \times 10^5$ kPa	
Yield curve	
Pressure (kPa)	Deviatoric stress (kPa)
$-1.149 \cdot 10^3$	6.2
6.88×10^3	6.2×10^3
1.0×10^{10}	6.2×10^3
Hydro tensile limit $p_{min} = -100$ kPa	

Table 2
Properties of Soil 2 and Soil 3.

Equation of State: Linear		
Strength: Drucker Prager		
Reference density $\rho = 2.2$ g/cm^3		
Bulk Modulus K	$K_2 = 2.2 \times 10^5$ kPa	$K_3 = 3.52 \times 10^5$ kPa
Shear Modulus G	$G_2 = 1.5 \times 10^5$ kPa	$G_3 = 2.4 \times 10^5$ kPa
Yield curve		
Pressure (kPa)	Deviatoric stress (kPa)	
-1.149×10^3	0	
6.88×10^3	6.2×10^3	
1.0×10^{10}	6.2×10^3	
Hydro tensile limit $p_{min} = -100$ kPa		

4 Effects of underground explosions on soils

4.1 Cratering

First, to check the ability of the numerical model, a test performed by Ambrosini and its colleagues (Ambrosini et al., 2002) is numerically simulated and the results are compared with experimental results. Then, the effect of varying the depth of the explosive on the dimensions and shape of craters is analyzed. Numerical results are also compared with experimental and empirical values.

All the tests were performed in soil with the following profile (Ambrosini et al., 2002):

(1) 0–0.70 m: brown clayey silt with organic matter.
(2) 0.70–5.0 m: reddish-brown clayey silt of low plasticity, classification CL, very dry.

Figure 2 shows the crater obtained experimentally for the case of a spherical explosive load of 10 kg of TNT buried 98 cm below the soil level (Ambrosini et al., 2002). The apparent crater diameter was D = 3.93 m. This case is first modeled and then, the depth is varied. The detonator is supposed to be in the center of the TNT spherical charge. Owing to the symmetry conditions, a two-dimensional (2D) axial symmetric mesh is used. A 5 m × 2.5 m nonuniform mesh representing a 5 m-diameter cylinder is defined

Please cite this article as: D. Ambrosini and B. Luccioni, Effects of underground explosions on soil and structures, Underground Space, https://doi.org/10.1016/j.undsp.2019.09.002

Table 3
Properties of Soil 4.

Reference density $\rho = 2.641$ g/cm^3
Hydro tensile limit $p_{min} = -1.00$ kPa
Equation of State: Shock Compaction with linear unloading
Strength: MO granular

Density-pressure curve		Density-sound speed curve		Yield curve		Density-shear modulus curve	
Density (g/cm^3)	Pressure (kPa)	Density (g/cm^3)	Sound Speed (m/s)	Pressure (kPa)	Deviatoric stress (kPa)	Density (g/cm^3)	Shear modulus (kPa)
1.674	0	1.674	2.652×10^2	0	0	1.674	7.69×10^4
1.739	4.577×10^3	1.745	8.521×10^2	3.40×10^3	4.23×10^3	1.746	8.69×10^5
1.874	1.498×10^4	2.086	1.722×10^3	3.49×10^4	4.47×10^4	2.086	4.03×10^6
1.997	2.915×10^4	2.147	1.875×10^3	1.01×10^5	1.24×10^5	2.147	4.91×10^6
2.144	5.917×10^4	2.300	2.265×10^3	1.85×10^5	2.26×10^5	2.300	7.77×10^6
2.250	9.809×10^4	2.572	2.956×10^3	5.00×10^5	2.26×10^5	2.572	1.48×10^7
2.380	1.794×10^5	2.598	3.112×10^3			2.598	1.66×10^7
2.485	2.894×10^5	2.635	4.600×10^3			2.635	3.67×10^7
2.585	4.502×10^5	2.641	4.634×10^3			2.641	3.73×10^7
2.671	6.507×10^5	2.800	4.634×10^3			2.800	3.73×10^7

Fig. 2. Experimental crater.

and is filled with the following materials: air, TNT, and soil (Fig. 3). The mesh is refined around the estimated final crater using 10 mm × 10 mm cells. Then, the dimensions of the numerical crater are obtained with errors of ±20 and ±10 mm of diameter and depth, respectively.

Material models described in Section 3.3 are used and Soil type 1 is adopted. The final crater is shown in Fig. 4. The numerical simulation gives an apparent crater diameter $D = 3.94$ m, which is almost equal to the apparent crater diameter measured in the test (Fig. 2).

Then, we varied the depth of burial of the explosive load from 25 cm to 3 m. The dimensions of the numerical models are modified to make them suitable for simulating the different depths of burial. The apparent crater diameters obtained are presented in Table 4. Consistent with the observations of Bull and Woodford (1999), the crater diameter increases with depth up to a certain threshold, above which the crater diameter decreases. A typical camouflet obtained for 10 kg of TNT buried at 3 m ($\lambda_c = 1.39$ m · kg$^{-\frac{1}{3}}$) is presented in Fig. 5.

The results presented in Table 4 are plotted in Fig. 6. Figure 6 also presents the experimental results obtained by Baker et al. (1991) and Ambrosini et al. (2002) and the numerical results obtained for the buried cylindrical explosives (Luccioni & Ambrosini, 2006). Although they correspond to different soil types and explosive shapes, a good agreement between the present numerical results and the experimental results by Baker et al. (1991) and Ambrosini et al. (2002) is observed in Fig. 6.

4.2 Landmines

In this section, a typical problem involving landmines is presented. Three field tests were conducted at the Detonics, Blast and Explosion Laboratory (DBEL) at Paardefontein Test Range, South Africa, each with an 8 kg TNT cylindrical charge. A schematic of the field test set-up is shown in Fig. 7(a). In Fig. 7(b) the 8 kg TNT charge for test 1 is shown before it was covered with 50 mm of soil. The charge had a 320 mm diameter and a diameter to height ratio of 5/1. A 100 g Pentolite booster was cast in the center to facilitate detonation. The numerical model is presented in Fig. 7(c) and the actual crater obtained is shown in Fig. 7(d).

The material models described in Section 3.3 are also used for this test and Soil type 1 is adopted. Moreover, both numerical Euler and Lagrange processors are used to model the soil. More details of the model, as well as the numerical model calibration, were presented by Luccioni et al. (2009).

The experimental crater diameter is reproduced first. The final state of the model with Euler and Lagrange processors is presented in Fig. 8. The apparent diameter of the craters obtained with the Euler and Lagrange processors are 2070 mm and 2060 mm, respectively. The mean crater diameter $D = 2065$ mm calculated numerically agrees with the apparent crater diameter $D = 1898$ mm measured in the

Please cite this article as: D. Ambrosini and B. Luccioni, Effects of underground explosions on soil and structures, Underground Space, https://doi.org/10.1016/j.undsp.2019.09.002

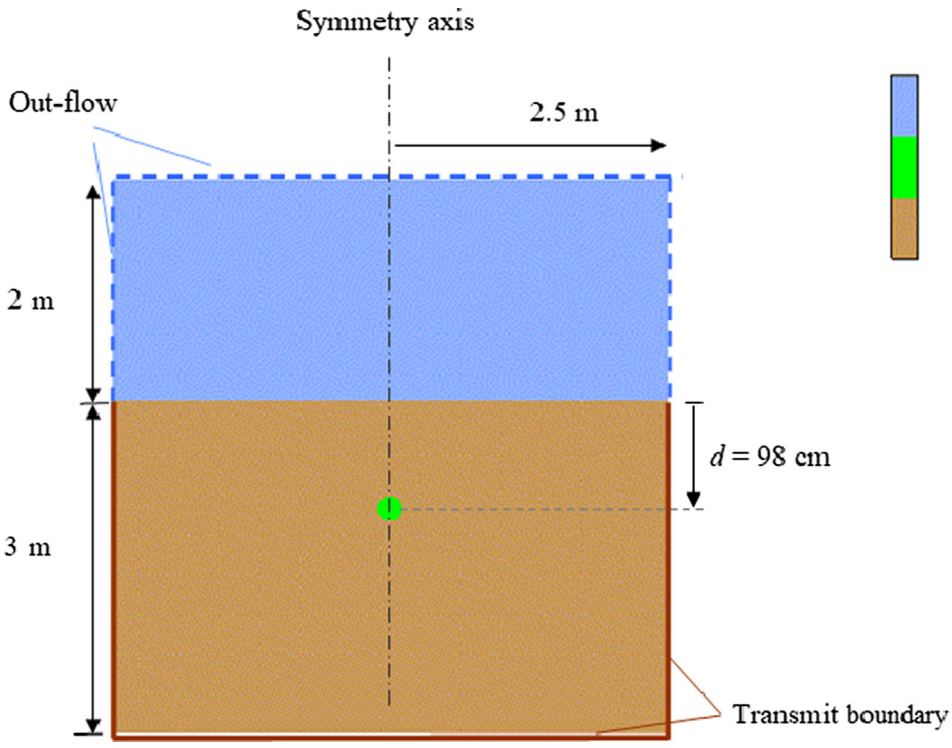

Fig. 3. Numerical model (10 kg of TNT at 98 cm depth).

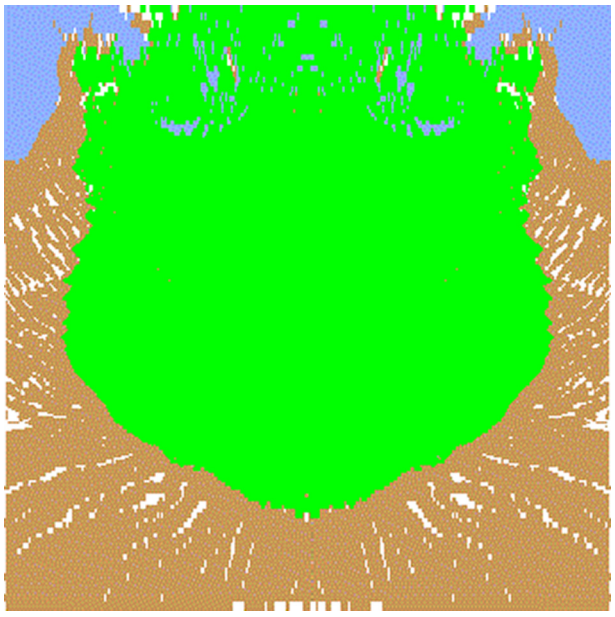

Fig. 4. Numerical crater (10 kg of TNT at 98 cm depth).

tests. The approximately 9% difference obtained is small for this type of studies considering the uncertainties involved.

The final shape of the crater obtained with the Euler processor resembles the actual one more accurately than that obtained with the Lagrange processor. After accurately reproducing the test, the diameters of the craters produced by different TNT masses located at different depths

Table 4
Craters produced by 10 kg of TNT at different depths.

d (m)	$\lambda_c = \frac{d}{W^{\frac{1}{3}}}\left(\mathrm{m}\cdot\mathrm{kg}^{-\frac{1}{3}}\right)$	Apparent crater diameter D (m)
0.25	0.116	2.40
0.50	0.232	3.78
1.00	0.464	3.94
2.00	0.928	4.30
3.00	1.392	3.58

are obtained using an Euler processor. A cylindrical explosive load of 0.26 kg or 8 kg of TNT with variable depth is used. The results for different scaled distances are presented in Table 5, where d represents the distance from the explosive charge mass center to the soil surface.

The results are plotted in Fig. 9 for comparison with the experimental results obtained by Baker et al. (1991) for alluvium soils and the results reported by Ambrosini et al. (2002) for spherical explosives buried in a reddish-brown clayey silt with low plasticity.

An excellent agreement between the numerical results obtained in this study and the experimental results for different soils types and explosive shapes obtained by Baker et al. (1991) and Ambrosini et al. (2002) is again observed.

The numerical results confirm that a function relating $D/2d$ and $W^{\frac{7}{24}}/d$ can be established. The tendency curve that best represents the numerical results is described by Eq. (2), in which the units are: W (kg), d (mm), and D (mm).

Please cite this article as: D. Ambrosini and B. Luccioni, Effects of underground explosions on soil and structures, Underground Space, https://doi.org/10.1016/j.undsp.2019.09.002

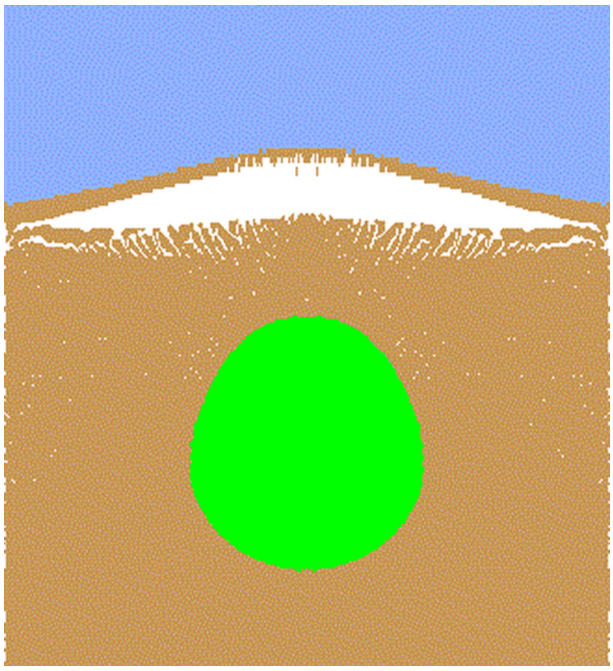

Fig. 5. Camouflet produced with 10 kg of TNT at a 3 m depth.

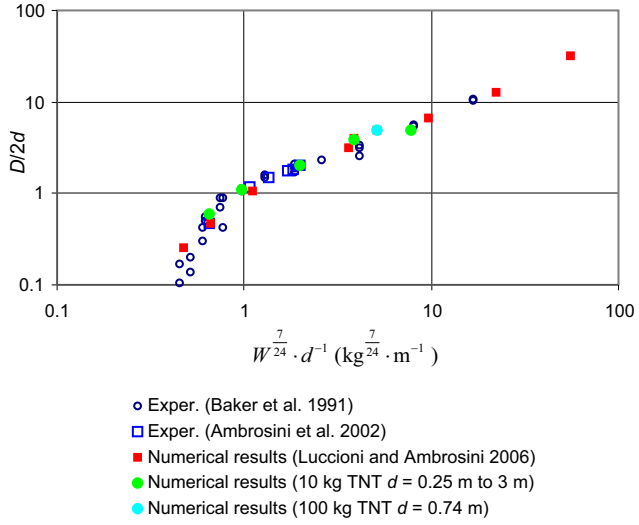

Fig. 6. Variation of crater diameter with scaled distance. Comparison with experimental results.

$$\log(D/(2d)) = 0.2993\left[\log\left(\frac{W^{\frac{7}{24}}}{d}\right)\right]^3 + 1.8562\left[\log\left(\frac{W^{\frac{7}{24}}}{d}\right)\right]^2 + 4.4913\log\left(\frac{W^{\frac{7}{24}}}{d}\right) + 4.7946 \quad (2)$$

4.3 Influence of overburden

The variation of the crater diameters with explosive depth obtained with Eq. (2) for different amounts of TNT is shown in Fig. 10, where the values of λ_c corresponding to the maximum crater diameter have also been indicated. It is clear that an optimum depth for which the crater is maximum can be defined and this value depends on the mass of the explosive. This result is coincident with the experimental observations of Ye (2008) for blast craters in rock.

4.4 Manholes

In this section, we consider the problem of explosives located in manholes (Ambrosini & Luccioni, 2012). The analysis of this problem is important for post-blast investigations of terrorist attacks in cities, in which the explosives can be located in manholes or other types of underground infrastructures.

The diameter of craters produced by 500 kg of TNT located in a manhole 1.7 m below ground with different types of covers was determined. A typical model for the case in which the explosive is not covered with soil and the resulting crater is illustrated in Fig. 11. The crater diameters obtained for the different cases simulated are presented in Table 6.

From the results in Table 6, it can be concluded that the nature of the cover of the manhole does not significantly affect the diameter of the crater. Moreover, if the manhole is open, the diameter of the crater is approximately 10% smaller.

5 Effects of underground explosions on structures

Different phenomena occurring as a result of the detonation of buried explosives that are responsible for the effect on structures above or under the ground are numerically simulated in this section.

5.1 Soil ejecta

Soil ejecta strongly influence the effect of buried explosions on targets located above the ground. The tests performed by Swinton and Bergeron (2004) are reproduced in this section. A steel container 800 mm in diameter and 500 mm deep was filled with dry medium sand. The mines were buried at the center of the container so that the top was 20 mm below the surface. A total of five tests were performed with buried mines. Three of these tests used PMN mines with 240 g of TNT, whereas in the other two, PMN mines with 200 g of PE4 were used.

Swinton and Bergeron (2004) presented radiographs of expanding detonation products. It took between 30 and 50 μs before any motion of the soil was visible. Then, the soil cap raised taking a hemispherical shape. The radiographs show a region of high density directly above the mine. The soil was compressed into a solid cap that broke soon thereafter. The vertical position of the front of the detonation products/soil ejecta was measured and the velocity was determined.

Please cite this article as: D. Ambrosini and B. Luccioni, Effects of underground explosions on soil and structures, Underground Space, https://doi.org/10.1016/j.undsp.2019.09.002

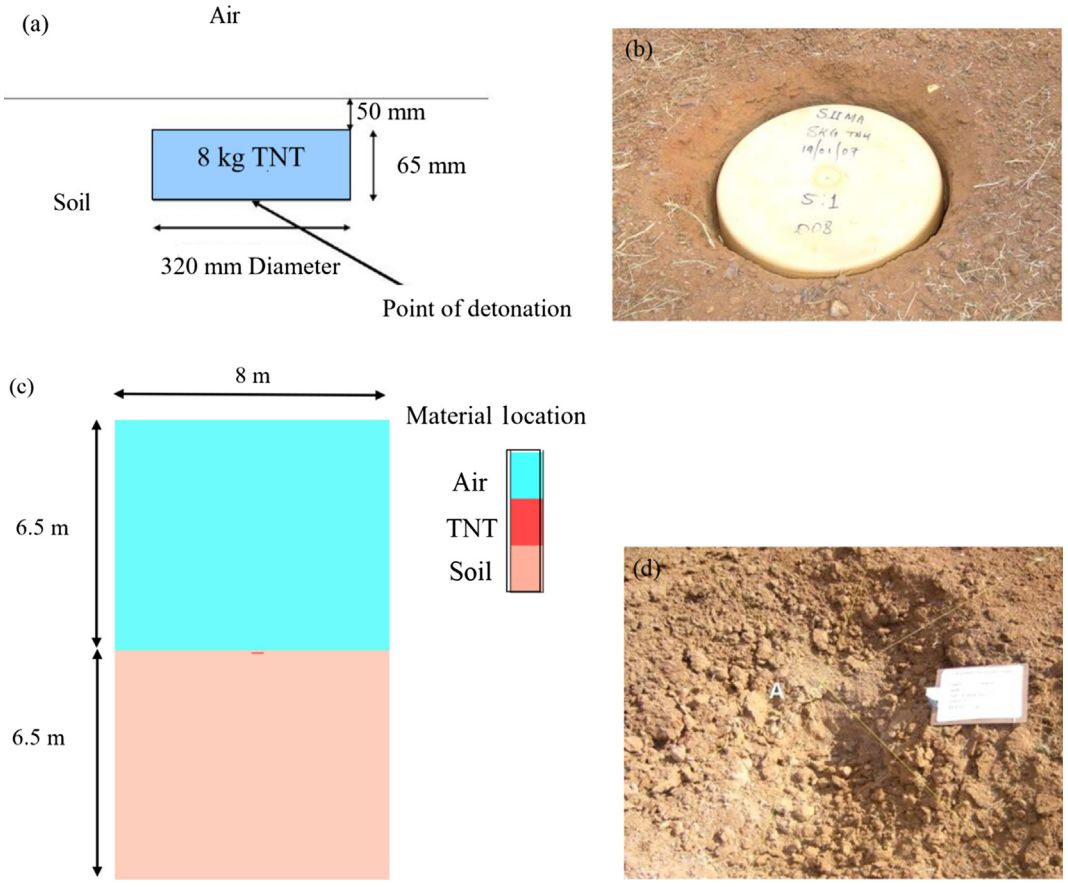

Fig. 7. (a) Typical problem set-up, (b) 8 kg TNT charge before the soil cover, (c) numerical model, and (d) actual crater.

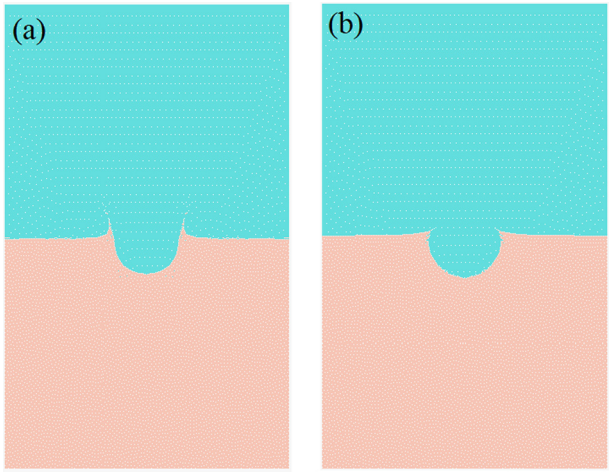

Fig. 8. Crater obtained with the (a) Euler processor and (b) Lagrange processor.

The model used to simulate these blast experiments is presented in Fig. 12. Although the entire model is shown, it is solved with an axial symmetric model owing to the symmetry of the problem. A total of 200 × 300 elements are used. The cells' dimensions are refined in the center of the model, where 2 mm × 2 mm elements are used. To represent the steel container, the soil is not allowed to flow in the soil limits, whereas the flow out of air is allowed in the upper part of the model.

Table 5
Crater diameter for different TNT masses and depths.

Mass of explosive W (kg of TNT)	Depth d (m)	Crater diameter D (mm)
8	0.032	2020
8	0.082	2070
8	0.20	2600
8	0.50	3120
0.26	0.60	1270
0.26	1.00	920
0.26	1.40	700

The four different models and soil properties described in Section 3.3 are used to model the soil. Figure 13 shows the soil ejecta numerically obtained with Soil 2 for the same time instants as those presented by Swinton and Bergeron (2004). It can be seen that the shape of the cap emerging from the soil is similar to that observed in the tests.

To compare the ability of different soil models to reproduce this problem, the vertical displacements and velocity of the top of soil ejecta are recorded for soils 1 to 4, and they are presented and compared with the experimental results in Table 7. Table 7 suggests that this sand can be

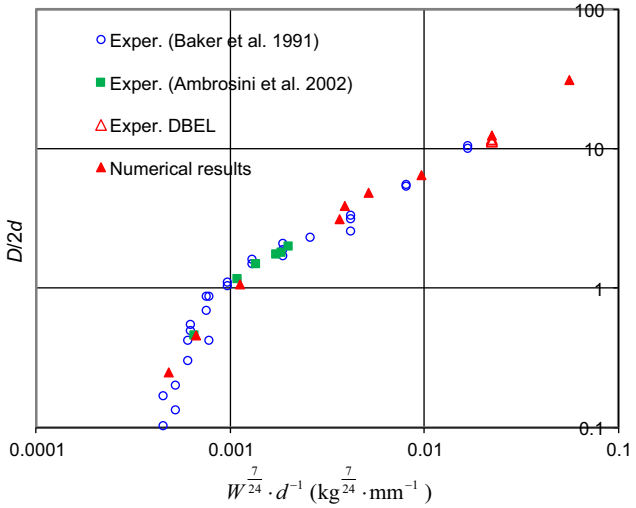

Fig. 9. Variation of crater diameter with scaled distance.

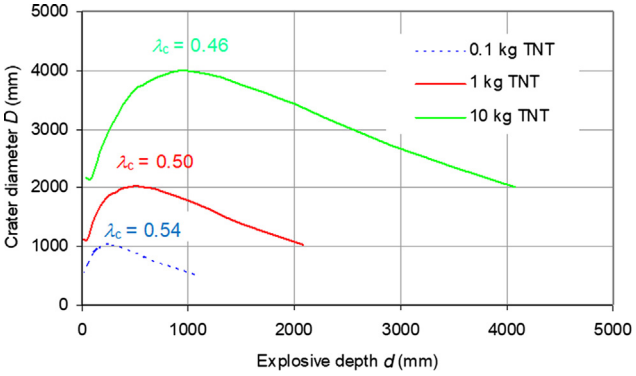

Fig. 10. Variation of crater diameter with overburden for different TNT masses.

modeled by Soil 2 or Soil 3, which approximately reproduce the vertical displacement and velocity of soil ejecta despite having strongly different stiffness.

5.2 Effects on aboveground targets

The blast tests reported by Hlady (2004) with landmines buried in engineered soil containers under controlled soil conditions are numerically simulated in this section. The energy transferred to a target attached to a piston mounted above the soil container was calculated using the height of the piston jump produced by the explosion. The thickness and diameter of the target plate were 25.4 mm and 254 mm, respectively; the total mass of the target plate including the mounting plate and the shaft was 47 kg. Different soils with different moisture contents were used. Cylindrical explosive charges corresponding to 25 g of C4, encased in plastic with a height-to-diameter ratio of 35%, were detonated in all tests. The overburden was varied from 0 to 150 mm. Hlady (2004) observed that the energy transfer produced by the landmines buried in high-density–high-moisture soil was seven times greater than that produced by the same explosive buried in dry sand and that an optimum overburden could be defined.

The 2D axial symmetry model used for the numerical simulation is shown in Fig. 14. The models and processors

Table 6
Crater diameter due to explosives located in manholes in different conditions.

Case	Apparent crater diameter D (m)
Cover with soil	9.2
Open manhole	8.4
Manhole with cover, pavement	9.4

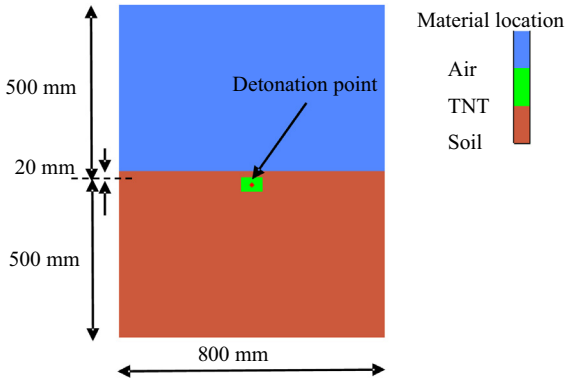

Fig. 12. Numerical model used to simulate the blast tests by Swinton and Bergeron (2004).

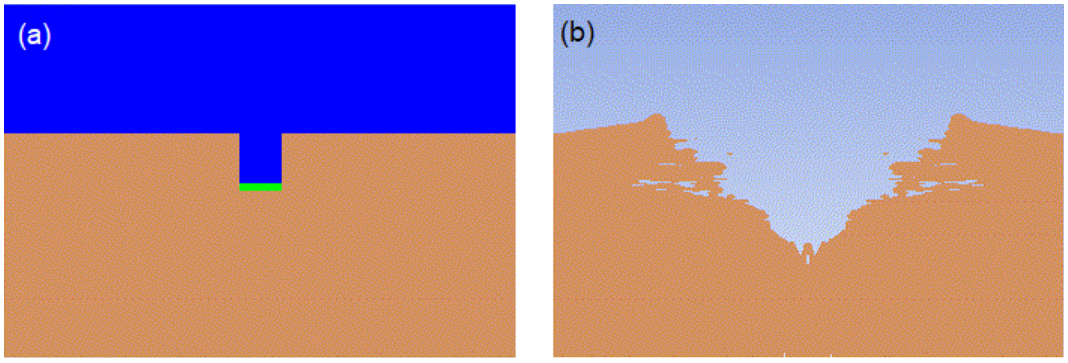

Fig. 11. Explosives in manholes. (a) Numerical model and (b) obtained crater.

Please cite this article as: D. Ambrosini and B. Luccioni, Effects of underground explosions on soil and structures, Underground Space, https://doi.org/10.1016/j.undsp.2019.09.002

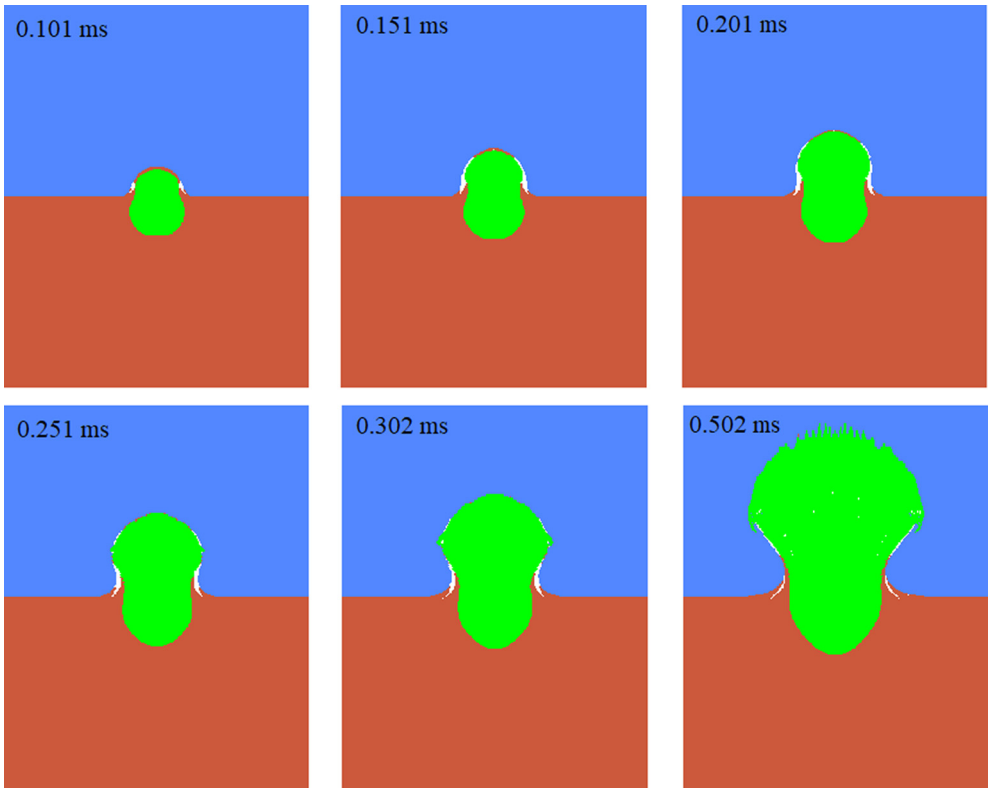

Fig. 13. Numerical simulation of detonation products expansion.

Table 7
Vertical displacement and velocities obtained for different types of soils.

Time (ms)	Displacement (mm)					Velocity (m/s)				
	Soil 1	Soil 2	Soil 3	Soil 4	Exper.	Soil 1	Soil 2	Soil 3	Soil 4	Exper.
0.101	100	76	78	98	80	1071	963	971	1207	820–926
0.151	153	125	125	159	110	1161	986	977	1209	
0201	206	172	172	219	175	1166	1001	1015	1182	
0.251	263	219	219	279	195	1171	928	1003	1158	
0.302	321	258	268	334	–	1027	954	1061	1138	

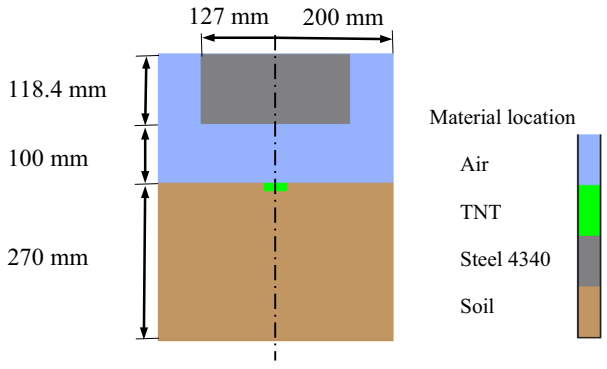

Fig. 14. Numerical model with 0 overburden.

described in Section 3 are used for the soil, air, and explosive. Considering a TNT equivalence of C4 approximately equal to 1.2 (TM5-855-1, 1984), the explosive charge is modeled as $W_{TNTequiv} = 30$ g of TNT detonated in the center of the bottom face.

Only a 400 mm diameter and 270 mm height soil cylinder representing the central upper part of the soil container is modeled. Flow-out boundary conditions are defined for the lateral and bottom border of the soil mesh to represent the surrounding soil. The target plate is modelled with the same diameter as that used in the experiments but with greater thickness to include the mass of the target plate, the mounting plate, and the shaft. A Lagrange processor is used for the plate and the Euler Lagrange interaction between air, explosive, and soil and the steel plate is considered. The stand-off distance of 100 mm is considered from the soil surface to the target plate. Two different types of soils, namely Soil 2 and Soil 3 with the properties defined in Table 2 are considered.

Please cite this article as: D. Ambrosini and B. Luccioni, Effects of underground explosions on soil and structures, Underground Space, https://doi.org/10.1016/j.undsp.2019.09.002

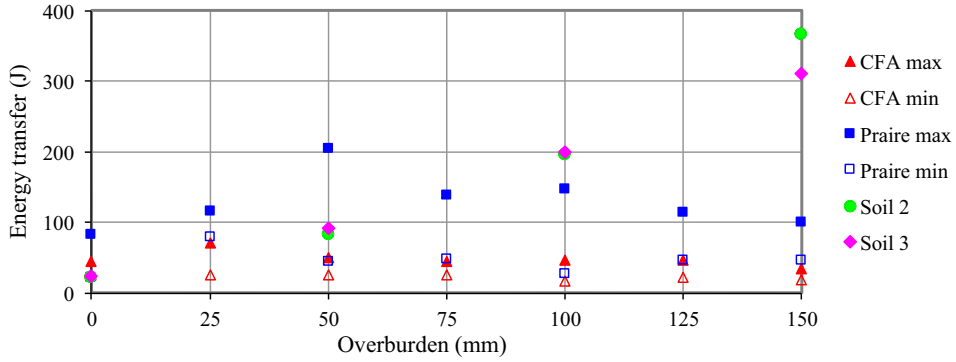

Fig. 15. Energy transfer to the target plate for different overburdens.

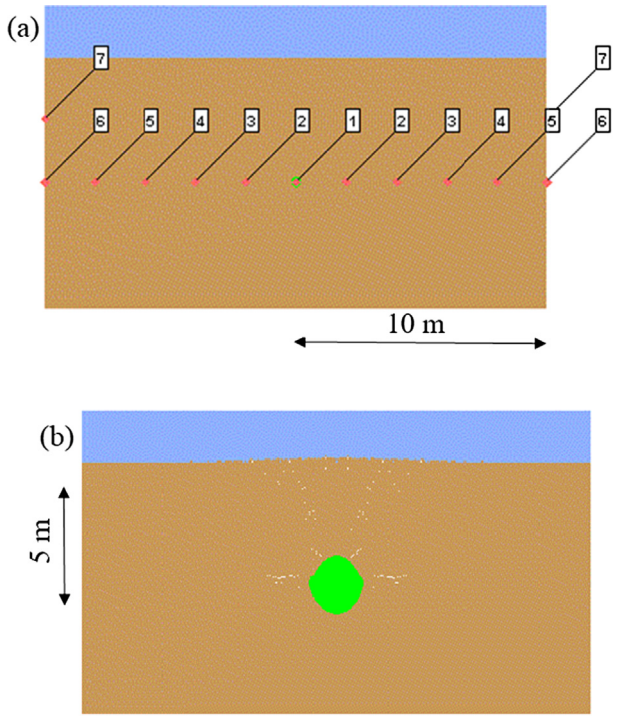

Fig. 16. Blast wave propagation in soil (50 kg of TNT at a 5 m depth). (a) Problem setup and (b) camouflet formed (107 ms).

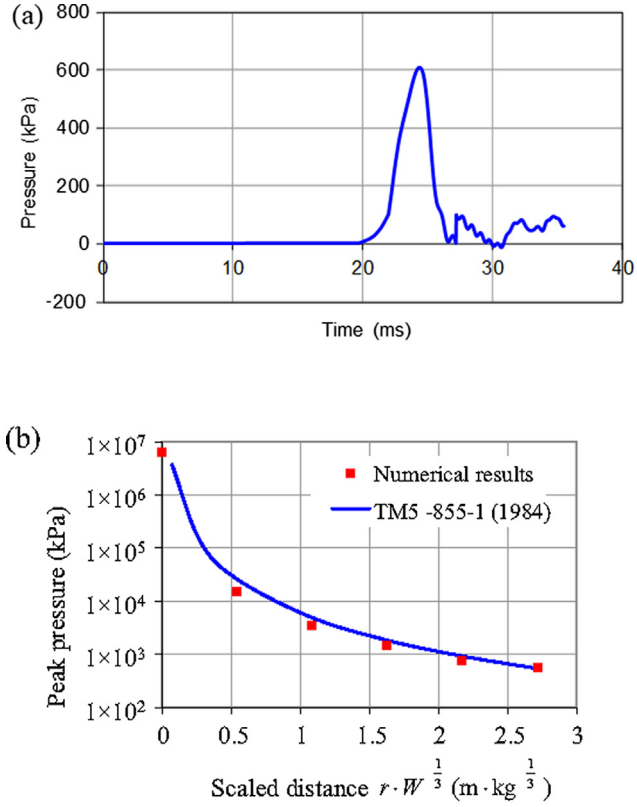

Fig. 17. Free-field blast wave propagation in soil. (a) Pressure history 10 m from the explosion and (b) peak pressure attenuation with distance from the blast.

The overburden h_0, which is the distance between the soil surface and the top of the explosive, is varied from 0 mm to 150 mm. The total energy transfer to the target plate obtained numerically for different overburdens is plotted in Fig. 15 for Soils 2 and 3 together with the experimental results by Hlady (2004).

The two types of soil modeled lead to energy transfer values similar to those reported by Hlady (2004) for small overburdens. For null overburden ($h_0 = 0$ mm), the value of the momentum transfer to the target plate is practically independent of the soil properties. For greater overburdens, Soil 3, which is stiffer than Soil 2, transmits more energy to the plate except for the case of 150 mm overburden.

Nevertheless, the great difference in stiffness between Soil 2 and Soil 3 produces only a small difference in energy transfer. The values of the energy transfer to the target plate obtained numerically for low overburdens up to 100 mm are in the same range as the experimental results reported by Hlady (2004). These results present a considerable dispersion. However, for $h_0 = 150$ mm, the numerical results are significantly higher than the experimental results. This difference is probably due to the energy loss from friction in the tests. The same problem was solved for Soils 1 and 4, but the results were significantly different

Please cite this article as: D. Ambrosini and B. Luccioni, Effects of underground explosions on soil and structures, Underground Space, https://doi.org/10.1016/j.undsp.2019.09.002

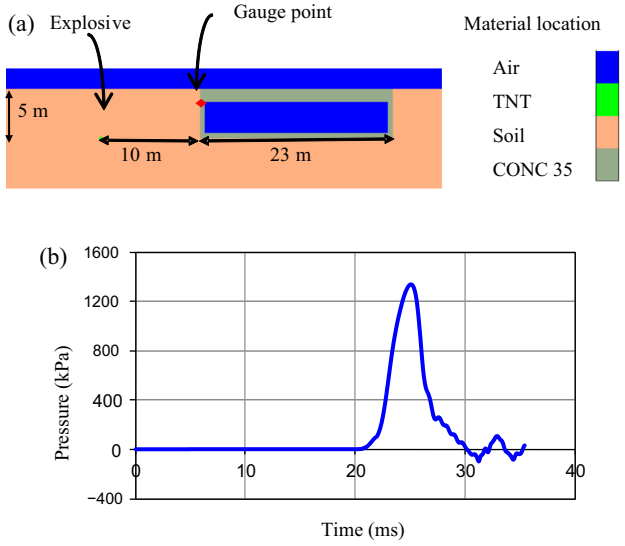

Fig. 18. Effect of 50 kg of TNT on a buried structure. (a) Problem setup and (b) pressure history in gauge point.

from the experimental results. The experimental results suggest that the optimum overburden is approximately 50–75 mm, but the corresponding maximum for the energy transfer could not be obtained with any of the soil models or parameters used.

5.3 Blast wave propagation in soil

The effects of buried explosions on underground structures are caused by the blast wave propagation in the soil and its interaction with the structure. In this section, the blast wave propagation in soil is analyzed numerically.

In particular, we simulate the explosion of a spherical charge consisting of 50 kg of TNT located 5 m beneath the ground. Based on the results obtained in the previous simulations, Soil 2 and Soil 3 are used. Flow-out boundary conditions are defined for all the soil borders. The model and the numerically obtained cavity are shown in Fig. 16 (a) and (b), respectively. The scaled depth is $\lambda_c = 1.36$ and as observed by Bull and Woodford (2004), a camouflet is formed.

The pressure and velocity values are recorded at the points indicated in Fig. 16(a). The pressure history at point 6 located 10 m away from the explosive charge is presented in Fig. 17(a). The values obtained numerically for the peak pressure and the blast wave arrival time are very close to those reported by Lu et al. (2005). Figure 17(b) shows the peak pressure attenuation with scaled distance and the curve representing the attenuation function suggested by TM5-855-1 (1984). A good agreement with this last function is observed. The problem was also solved for Soils 1, 3, and 4. As expected, a strong dependence of the blast wave on the soil model and parameters was observed.

5.4 Effect of buried explosions on underground structures

In this section, we analyze the effect of a buried explosion on a reinforced concrete structure (Lu et al., 2005). The explosive position and mass are the same as those in the previous section. The model is presented in Fig. 18 (a), where the location of the explosive and the gauge point are indicated. The air, soil, and explosive load are simulated with a Euler multi-material processor, whereas a Lagrange processor is used for the reinforced concrete structure. The interaction between Euler and Lagrange meshes is activated.

For the concrete, we used an RHT model with the properties available in AUTODYN material library and a concrete strength of 35 MPa and an instantaneous geometric strain erosion limit of 0.01. The main properties are shown in Tables 8 and 9.

The reflected pressure time-history for a gauge point located in the center of the structure's front face is shown in Fig. 18(b). The curve shows multiple reflections of the blast wave on the concrete structure. The values of the peak pressure, arrival time, and duration of the positive phase are similar to those obtained by Lu et al. (2005) with a 2D model using a combination of SPH and FEM simulation and a more complex soil model.

Table 9
RHT damage model: default parameter setting.

D_1	D_2	e^{fail}_{min}	G_{fail}/G
4×10^{-2}	1	1×10^{-2}	1.3×10^{-1}

Notes: G_{fail}/G is the residual shear modulus fraction.

Table 8
RHT strength model: default parameter setting.

G (kPa)	f'_c(kPa)	f_t/f'_c		f_s/f'_c	A		N
1.09×10^7	3.5×10^4	0.1		0.18	1.6		6.1×10^{-1}
$Q_{2.0}$	B_Q		$\frac{G_{elast}}{G_{elast}-G_{plas}}$	$f_{t,el}/f_t$		$f_{c,el}/f'_c$	B
6.805×10^{-1}	1.05×10^{-2}		2	0.7		0.53	1.6
m	α	δ					
6.1×10^{-1}	3.2×10^{-2}	3.6×10^{-2}					

Notes: G is shear modulus, f_s is shear strength, and $\frac{G_{elast}}{G_{elast}-G_{plas}}$ is the hardening slope.

Please cite this article as: D. Ambrosini and B. Luccioni, Effects of underground explosions on soil and structures, Underground Space, https://doi.org/10.1016/j.undsp.2019.09.002

6 Conclusions

The numerically obtained dimensions of the craters and camouflets are very close to the experimental results reported by other researchers. It was shown that the diameter of the crater is almost independent of the soil type and the explosive shape for similar aspect ratios. Nevertheless, it is clear that the depth of the craters obtained is greater than the apparent depth observed in experimental tests. Numerical results indicate that the optimal scaled depth for which the maximum crater diameter can be obtained is in the range defined by $0.4\,\mathrm{m}\cdot\mathrm{kg}^{-\frac{1}{3}} < \lambda_c < 0.6\,\mathrm{m}\cdot\mathrm{kg}^{-\frac{1}{3}}$ (Fig. 10).

The main issues concerning blast wave propagation in soil (peak pressure, arrival time, attenuation with distance) could be accurately simulated by reproducing experimental results reported by other authors and are in accordance with values suggested by codes. However, the results are strongly dependent on the soil model and properties. This indicates the importance of a careful soil characterization and an adequate soil model usage when assessing the behavior of underground structures subjected to buried explosions. For this purpose, underground structures must be explicitly modeled. The differences observed in the reflected pressure values can be attributed to the simplicity of the model used in this study.

The effect of underground explosions on objects placed above the ground also depends on the soil properties. The influence of soil properties is practically negligible for null overburden, but it increases as the overburden of the explosive load increases. The results obtained for the soil models analyzed are comparable to experimental results for small overburdens up to 100 mm. A considerable difference between numerical and experimental results is obtained for the highest overburden analyzed. This difference can be attributed to both the soil model and the Euler multi-material processor used for the soil, which is not able to reproduce the actual soil ejecta.

Further research, including soil models and processor is needed in the area of underground explosions and their effect on structures above and under the ground.

Conflict of interest

There is no conflict of interest.

Acknowledgments

The authors wish to thank the help received from Amelia Campos for the English revision. The financial support of the CONICET (Argentina) and National Universities of Cuyo and Tucumán is gratefully acknowledged. Special acknowledgements are extended to the reviewers of the first version of the paper because their useful suggestions led to improvements of the work.

References

Alia, A., & Souli, M. (2006). High explosive simulation using multi-material formulations. *Applied Thermal Engineering, 26*(10), 1032–1042.

Ambrosini, D., & Luccioni, B. (2012). Craters produced by explosions on, above and under the ground. In H. Hao, & Z.-X. Li (Eds.), *Chapter 13 of the book: Advances in protective structures research* (pp. 365–396). London UK: CRC Press/Balkema. Taylor & Francis Group.

Ambrosini, D., Luccioni, B., Danesi, R., Riera, J., & Rocha, M. (2002). Size of craters produced by explosive charges on or above the ground surface. *Shock Waves, 12*(1), 69–78.

An, J., Tuan, C. Y., Cheeseman, B. A., & Gazonas, G. A. (2011). Simulation of soil behavior under blast loading. *International Journal of Geomechanics, 11*(4), 323–334.

ANSYS AUTODYN V18.1. (2017). Explicit software for non-linear dynamics. User's manual..

Baker, W. E., Cox, P. A., Westine, P. S., Kulesz, J. J., & Strehlow, R. A. (1983). Explosion hazards and evaluation. Amsterdam: Elsevier.

Baker, W. E., Westine, P. S., & Dodge, F. T. (1991). Similarity methods in engineering dynamics. Amsterdam: Elsevier.

Bergeron, D., Walker, R., & Coffey, C. (1998). Detonation of 100-gram anti-personnel mine surrogate charges in sand – a test case for computer code validation. Technical report 668. Ralston, Alberta, Canada: Defence Research Establishment Suffield.

Bull, J. W., & Woodford, C. H. (2004). Fatigue life of subgrade in the cone of disturbance following an underground explosion. *Computers and Structures, 82*(23/24/25/26), 2041–2048.

Bull, J. W., & Woodford, C. H. (1998). Camouflets and their effect on runway support. *Computers and Structures, 69*(6), 695–706.

Bull, J. W., & Woodford, C. H. (1999). The effects of camouflets on subgrade surface support. *Computers and Structures, 73*(1/2/3/4/5), 315–325.

Cheeseman, B. A., Wolf, S., Yen, C. F., & Skaggs, R. (2006). Blast simulation of explosives buried in saturated sand. *Fragblast, 10*(1/2), 1–8.

Chen, J. Y., & Lien, F. S. (2018). Simulations for soil explosion and its effects on structures using SPH method. *International Journal of Impact Engineering, 112*, 41–51.

Clarke, S. D., Rigby, S. E., Fay, S. D., Tyas, A., Reay, J. J., Warren, J. A., ... Elgy, I. (2015). 'Bubble-type' vs 'shock-type' loading from buried explosives. *Proceedings of the 16th international symposium on interaction of the effects of munitions with structures (ISIEMS16), Florida, USA*.

Denefeld, V., Heider, N., & Holzwarth, A. (2017). Measurement of the spatial specific impulse distribution due to buried high explosive charge detonation. *Defence Technology, 13*(3), 219–227.

Fan, H., & Li, S. A. (2017). Peridynamics-SPH modeling and simulation of blast fragmentation of soil under buried explosive loads. *Computer Methods in Applied Mechanics and Engineering, 318*, 349–381.

Fourney, W. L., Leiste, H. U., Haunch, A., & Jung, D. (2010). Distribution of specific impulse on vehicles subjected to IED's. *Proceedings of the IMPLAST 2010 conference, Rhode Island, USA*.

Grujicic, M., & Pandurangan, B. (2008). A combined multi-material Euler/Lagrange computational analysis of blast loading resulting from detonation of buried landmines. *Multidiscipline Modeling in Materials and Structures, 4*(2), 105–124.

Grujicic, M., Pandurangan, B., & Cheeseman, B. A. (2006). The effect of degree of saturation of sand on detonation phenomena associated with shallow-buried and ground-laid mines. *Shock and Vibration, 13*(1), 41–61.

Hlady, S. L. (2004). Effect of soil parameters on land mine blast. *18th military aspects of blast and shock conference, MABS18, Germany*.

Hu, D., Long, T., Liu, C., Yang, G., & Han, X. (2014). Swelling movement induced by underground explosion of aluminized explosive in multilayered compact material. *International Journal of Rock Mechanics & Mining Sciences., 71*, 330–339.

Jayasinghe, L., Thambiratnam, D., Perera, N., & Jayasooriya, J. (2013). Computer simulation of underground blast response of pile in saturated soil. *Computers & Structures, 120*, 86–95.

Kinney, G., & Graham, K. (1985). *Explosive shocks in air* (2nd ed.). Springer-Verlag.

Lu, Y., Wang, Z., & Chong, K. (2005). A comparative study of buried structure in soil subjected to blast load using 2D and 3D numerical

Please cite this article as: D. Ambrosini and B. Luccioni, Effects of underground explosions on soil and structures, Underground Space, https://doi.org/10.1016/j.undsp.2019.09.002

simulations. *Soil Dynamics and Earthquake Engineering, 25*(4), 275–288.

Luccioni, B., & Ambrosini, D. (2006). Craters produced by underground explosions. *Computational Mechanics, XXV*, 1603–1614.

Luccioni, B., Ambrosini, D., Nurick, G., & Snyman, I. (2009). Craters produced by underground explosions. *Computers and Structures, 87*, 1366–1373.

Rigby, S. E., Fay, S. D., Clarke, S. D., Tyas, A., Reay, J. J., Warren, J. A., et al. (2016). Measuring spatial pressure distribution from explosives buried in dry Leighton Buzzard sand. *International Journal of Impact Engineering, 96*, 89–104.

Rigby, S. E., Fay, S. D., Tyas, A., Clarke, S. D., Reay, J. J., Warren, J. A., et al. (2018). Influence of particle size distribution on the blast pressure profile from explosives buried in saturated soils. *Shock Waves, 28*(3), 613–626.

Smith, P. D., & Hetherington, J. G. (1994). *Blast and ballistic loading of structures*. Great Britain: Butterworth-Heinemann Ltd.

Swinton, R. J., & Bergeron, D. M. (2004). Evaluation of a silent killer, the PMN anti-personnel blast mine. DSTO-TR-1582, AR-013-112, Technical report.

TM5-855-1 (1984). *Fundamental of protective design for conventional weapons*. Vicksburg: US Army Engineer Waterways Experiment Station.

Wang, Z., Hao, H., & Lu, Y. (2004). The three-phase soil model for simulating stress wave propagation due to blast loading. *International Journal for Numerical and Analytical Methods in Geomechanics, 28*(1), 33–56.

Wang, Z., Lu, Y., Hao, H., & Chong, K. (2005). A full coupled numerical analysis approach for buried structures subjected to subsurface blast. *Computers and Structures, 83*(4/5), 339–356.

Wang, M., Qiu, Y., & Yue, S. (2018). Similitude laws and modeling experiments of explosion cratering in multi-layered geotechnical media. *International Journal of Impact Engineering, 117*, 32–47.

Wu, C., & Hao, H. (2005). Numerical study of characteristics of underground blast induced surface ground motion and their effect on above-ground structures. Part I. Ground motion characteristics. *Soil Dynamics and Earthquake Engineering, 25*(1), 27–38.

Wu, C., Hao, H., Lu, Y., & Sun, S. (2004). Numerical simulation of structural responses on a sand layer to blast induced ground excitations. *Computers and Structures, 82*, 799–814.

Yankelevsky, D. Z., Karinski, Y. S., & Feldgun, V. R. (2011). Re-examination of the shock wave's peak pressure attenuation in soils. *International Journal of Impact Engineering, 38*(11), 864–881.

Ye, T. Q. (2008). Field experiment for blasting crater. *Journal of China University of Mining and Technology, 18*(2), 224–228.

Please cite this article as: D. Ambrosini and B. Luccioni, Effects of underground explosions on soil and structures, Underground Space, https://doi.org/10.1016/j.undsp.2019.09.002